CATALYTIC ACTIVITY OF CHEMICAL AND BIOLOGICAL NANOSILVER: A COMPARATIVE STUDY

[1]Dr. Richa Singh & [2]Bhumika B. Jain
[1]Assistant Professor, [2]PG Scholar
Department of Biotechnology,
SIES College of Arts, Science and Commerce, Sion (W), Mumbai - 22, India

Abstract: ***Dyes are used in various industries and laboratories as coloring agents. However, their unregulated disposal in environment poses a major threat for human health, plants and ecological balance. Hence, novel strategies are required for efficient decolorization and degradation of these synthetic dyes. Silver nanoparticles (SNPs) exhibit an excellent catalytic activity in organic reactions. The present study deals with synthesis, optimization and nanocatalytic activity of SNPs. Here, we have synthesized SNPs by two ways: chemical reduction using trisodium citrate and biological synthesis using Murraya koenigii leaf extract. Reaction parameters, such as silver nitrate concentration and temperature affected the rate of synthesis and morphology of SNPs. The nanoparticles were roughly spherical and crystalline with face-centered cubic structure. We further compared their nanocatalytic activity with respect to dye decolorization and found that plant mediated SNPs exhibit faster decolorization of congo red and trypan blue as compared to chemically synthesized SNPs. This is the first study to compare chemical and biological nanosilver for dye decolorization catalysis.***

Index Terms – silver nanoparticles, nanocatalyst, congo red, trypan blue

---

I. INTRODUCTION

A dye is a colored substance having affinity for the substrate to which it is being applied. It usually consists of a chromophore, which imparts color, and an auxochrome. Dyes and stains have become a part of our daily life. These are used in various laboratories and industries such as food, fabric, paper, pulp, printing, painting, leather, plastic, cosmetics, pharmaceuticals, etc. [1-3]. Annual worldwide consumption of dyes and pigments is approximately 7×10^5 tons; out of which, about two-third is utilized by textile industry [4]. Inefficiency in the coloring generates large amount of dye residues, which are released in water or dumped on soil, leading to severe environmental pollution, disruption of ecological balance and disturbance in aquatic system. The toxic effect of dyes is not limited to marine organisms but also reported in plants and animals [5,6]. The effluent contains variety of synthetic dyes, such as azo, azine, direct, reactive and vat dyes, which are toxic, mutagenic and carcinogenic in nature [7]. Triphenylmethane dyes, crystal violet and malachite green, have been reported as recalcitrant molecules, which persist for a long time in environment. They act as mitotic poisons and potent carcinogens in some species of fish [8]. Congo red, an anionic azo dye, is known to cause allergic reactions. Its metabolism to the compound benzidine can cause human cancer [9,10]. There are evidences against trypan blue (azo dye), safranin (azine dye) and methylene blue (thiazine dye) causing carcinogenicity in animals [11-13].

Synthetic dyes are very difficult to remove because of their complex aromatic structures that provide them high stability [14]. Physical and chemical methods of dye degradation include adsorption, ion exchange, lime coagulation, membrane separation, reverse osmosis, advanced oxidation process etc. These methods are capital-intensive and produce large heaps of wastes [15]. Recently, biological routes involving microbial degradation, biosorption and decolorization have been considered; however, their feasibility is limited owing to requirement of a large land area and sensitivity to diurnal variation. Moreover, azo dyes are resistant to microbial degradation [16]. Anaerobic reduction of azo dyes by microbes leads to the formation of carcinogenic aromatic amines [17]. Hence, there is a high need to search more feasible method of dye decolorization/degradation, one of which is nanocatalysts.

Nanoparticles exhibit excellent catalytic activity for organic reactions mainly involving electron transfer reactions [18,19]. Smaller size increases their fermi potential leading to a decrease in activation energy, thereby, increasing the rate of chemical reaction [20]. Besides this, other advantages of nanocatalysts are insolubility in reaction medium, high dispersity and ease of separation. Silver nanoparticles (SNPs) can catalyze C-C, C-N, C-O, C-S coupling reactions, organic transformations and redox reactions [14]. They are also known to catalyze the reduction of 4-nitrophenol and methylene blue [21-23]. It has been suggested that high surface area to volume ratio renders SNPs with more catalytic sites for chemical reactions [24].

Chemical reduction of silver salt is one of the common methods to produce SNPs at low cost and in high yield. It involves three components – (i) metal precursors, (ii) reducing agents, such as trisodium citrate, sodium borohydride, ethylene glycol, cetyltrimethylammonium bromide, hydrazine hydrae, hydroquinone, etc. and (iii) stabilizing or capping agents, such as sodium citrate, sodium oleate, polyvinylpyrrolidone and polyvinyl alcohol [25,26]. Though the method is simple and convenient, harsh conditions are required to facilitate the reduction of silver ions to SNPs. In view of these disadvantages, synthesis of SNPs using plant and plant extract has gained significance [27]. These methods are considered to be nontoxic, ecofriendly and biocompatible over chemical methods. No additional stabilizing agent is required. Moreover, it has been suggested that biological nanoparticles exhibit greater activity as compared to chemically synthesized nanoparticles [24]. Therefore, in pursuit of developing novel dye decolorization formulation, we have directed our efforts to screen SNPs, synthesized through chemical and biological approaches, for their feasibility as nanocatalysts.

II. EXPERIMENTAL PROCEDURE

2.1 Chemicals

Silver nitrate ($AgNO_3$) and sodium borohydride ($NaBH_4$) were obtained from HiMedia (Mumbai, India). Trisodium citrate, congo red, crystal violet, methylene blue, malachite green, safranin and trypan blue were procured from Loba Chemie Pvt Ltd India.

2.2 Synthesis of chemical SNPs (CSNPs)

For synthesis of CSNPs, Turkevich method was employed. In brief, 1 mM sodium citrate was mixed with 1 mM $AgNO_3$ solution in a reaction volume of 10 ml. The reaction mixture was kept in water bath at 70˚C for 2h. The synthesis of CSNPs was identified by a change in the color of the solution.

2.3 Synthesis of SNPs by plant extract (PSNPs)

Fresh leaves of *Murraya koenigii* (curry leaves) were obtained from a curry leaf plant in Virar. The leaves were washed thoroughly with distilled water to remove the dust particles and then were dried for 4-5 days at room temperature without any exposure to sunlight. The dried leaves were pulverized into fine powder using mixer grinder. To prepare extract, 5 g of the powder was added to a flask containing 100 ml of distilled water with a tight cotton plug. The mixture was boiled for 15 min, cooled and filtered using Whatman filter paper No.1 to obtain plant extract. The extract was stored at 4ºC.

For synthesis of PSNPs, 0.5 ml of leaf extract was added to 1 mM $AgNO_3$ solution in a reaction volume of 10 ml and incubated at 40ºC in water bath (Equitron Medica, Mumbai, India) for 2h. The synthesis of PSNPs was identified by a change in the color of the solution.

2.4 Optimization of $AgNO_3$ concentration

In order to obtain the optimum concentration of $AgNO_3$, different concentrations of $AgNO_3$ (in mM) i.e. 0.3, 0.5, 1.0, 3.0, 5.0 were added to the tubes containing 0.5 ml leaf extract (for PSNPs) and 1 mM trisodium citrate (for CSNPs). The tubes were further incubated for 2h at 40˚C and 60˚C, respectively. The synthesis of both PSNPs and CSNPs was monitored by taking absorbance using a UV-visible spectrophotometer (Equip-Tronics EQ-825A, Mumbai, India).

2.5 Optimization of temperature

To optimize the incubation temperature, optimum concentration of $AgNO_3$ was added in the tubes containing 0.5 ml plant extract (for PSNPs) and 1mM trisodium citrate (for CSNPs). The tubes were incubated at different temperatures ranging from 30 to 80˚C for 2h. The synthesis was monitored by reading absorbance using a UV-visible spectrophotometer.

2.6 Characterization

UV-Vis spectrum analysis was performed using UV-visible spectrophotometer before and after optimization of reaction parameters for PSNPs and CSNPs using 350 to 600 nm wavelength range. SNP samples for TEM were prepared by drop-coating the SNP solution on carbon-coated copper grid and drying. The analyses were performed on FEI Tecnai G^2 12 Bio Twin (The Netherlands) TEM. The size of SNPs was estimated using ImageJ software. SAED pattern of a randomly selected particle from the two samples were obtained by inserting a thin strip of metal, for diffraction, through a selected area aperture present in the TEM.

2.7 Screening of dyes for nanocatalytic activity of SNPs

In primary screening, six dyes i.e. congo red, crystal violet, methylene blue, malachite green, safranin and trypan blue at concentration of 0.05 mg/ml were observed for complete decolorization by adding 1 mg/ml SNPs with 3.5 mg/ml $NaBH_4$. Suitable controls were also maintained for each dye.

2.8 Effect of SNP concentration on dye decolorization

Dyes giving positive results with combination of SNPs and $NaBH_4$ were used for time course studies. SNPs were added at different concentrations (mg/ml) i.e. (1, 0.5, 0.1, 0.05, 0.01, 0.005 and 0.001) and the time required for complete decolorization was monitored.

2.9 UV-Visible spectroscopy

UV-visible spectroscopic analysis was carried out to study the dye decolorization kinetics with combination of SNPs and $NaBH_4$. UV-visible spectrum in the range of 350 to 700 nm was taken at regular time intervals of 10min.

III. RESULTS AND DISCUSSION

3.1 Synthesis of SNPs

For synthesis of PSNPs, $AgNO_3$ solution was mixed with extract of curry leaves. A visible color change from pale yellow to reddish brown was observed in the reaction mixture after incubation at 40˚C for 2h (Figure 1A). The tube containing trisodium citrate and $AgNO_3$ turned yellow from colorless at 70˚C. This color change indicates the synthesis of PSNPs and CSNPs [28]. The intensity of color increased with reaction time, after which no further color change was observed. This suggested the complete reduction of silver ions to nanosilver [29]. No color change was observed in the control tube.

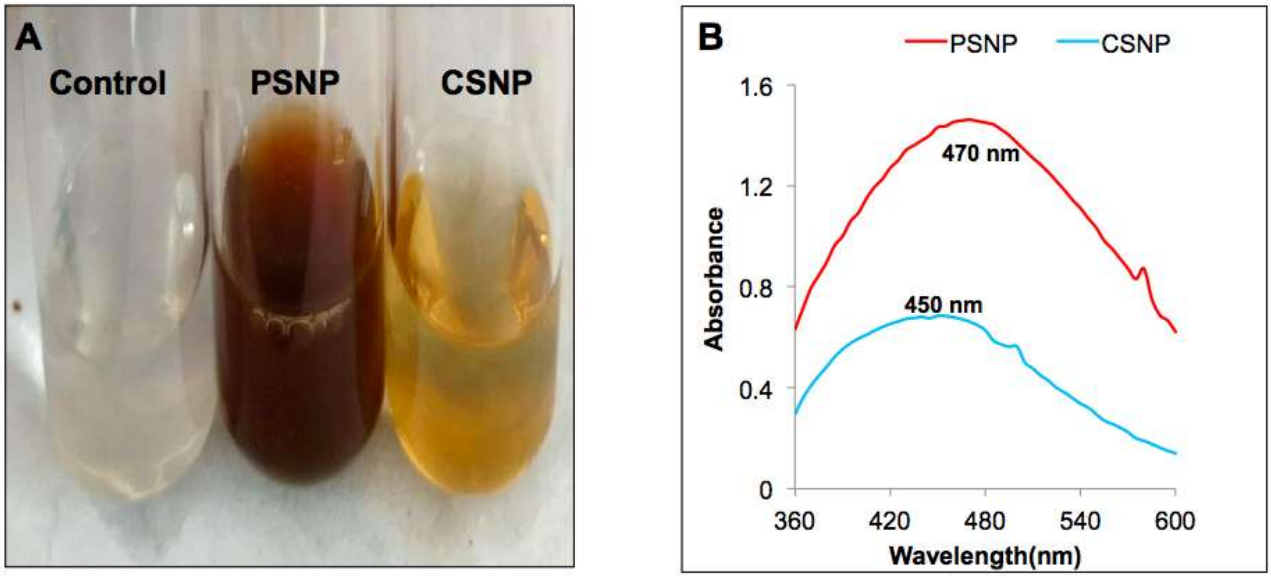

Figure 1. Preliminary synthesis of PSNPs and CSNPs. (A) Color change in the reaction mixture. (B) UV-visible spectrum of PSNPs and CSNPs showing SPR peak.

Bioreduction of Ag^+ ions to Ag^0 is a complex phenomenon involving biomolecules like enzymes, proteins, flavonoids, phenols, vitamins, organic acids, amino acids and polysaccharides [24,30,31]. Curry leaves are known to contain vast array of biomolecules such as lutein, tocopherol, carotene, carbazole, alkaloids, murrayazoline, murrayazolidine, murrayanl, koenimbine, mahnine, isomahnine, bismahnine, euchrstine and bispyrafoline, which can act as reducing and stabilizing agents for PSNPs [32]. Trisodium citrate is one of the common reducing agents employed for chemical synthesis of metal nanoparticles [33]. Citrate brings about the reduction of silver; Ag^+ is reduced to Ag^0. The reaction to prepare CSNPs can be expressed as:

$$4Ag^+ + C_6H_5O_7Na_3 + 2H_2O \rightarrow 4Ag^0 + C_6H_5O_7H_3 + 3Na^+ + H^+ + O_2$$

In UV-visible spectrum, a single peak was observed at 470 nm for PSNPs and at 450 nm for CSNPs (Figure 1B). In plasmonic metal nanoparticles, like SNPs, electrons move freely because of close proximity of conduction and valence bands [34]. When excited with a light of specific wavelength, there is a collective oscillation of conduction band electrons giving rise to a resonance, known as surface plasmon resonance (SPR). This SPR is represented by a SPR peak in UV-visible spectrum, which is usually located between 410 to 470 nm for SNPs of size ranging from 2 to 100nm. It is also the origin of the observed color change during nanoparticle formation [35]. Characteristics of an SPR peak can be used to study properties of nanoparticles [36]. According to Mie's theory, only a single SPR peak is expected for spherical metal nanoparticles, whereas anisotropic particles can give rise to two or more peaks depending upon their morphology [37]. For rod-like SNPs, two SPR bands arise from the excitation of longitudinal and transversal plasmonic vibrations [38]. In present study, a single SPR peak is observed for both PSNPs and CSNPs, which suggests that our SNPs are spherical in shape.

3.2 Optimization of reaction parameters

Optimization has been suggested to play a major role in shape-controlled synthesis, aggregation and stability of nanoparticles [28]. In present study, significant effects of reaction parameters were observed on the rate of synthesis of SNPs during optimization, which was monitored by measuring absorbance at regular intervals.

3.2.1 $AgNO_3$ concentration

To determine the optimum concentration of $AgNO_3$ for maximum synthesis, different concentration of $AgNO_3$ was added to leaf extract and trisodium citrate and incubated for 2h at 40˚C and 70˚C, respectively. At a fixed incubation temperature, increase in SNPs synthesis was observed with increasing $AgNO_3$ concentration in the reaction mixture. Maximum synthesis of nanoparticles occurred at 5 mM followed by 3 mM silver salt concentration (Figure 2). Lower concentrations showed lesser reduction of silver ions to nanoparticles. According to a report, a reaction with 6 ml of plant extract added to 1 mM $AgNO_3$ gave synthesis of PSNPs in 30 min [39]. In our study, we have used only 0.5 ml of leaf extract for PSNPs. This suggested that the key biomolecules responsible for reduction are present in higher amount in our leaf extract, which is also corroborated by the need of higher silver salt concentration for maximum synthesis. Godet et al. employed 6 mM trisodium citrate and 2 mM $AgNO_3$ as optimum concentration of reactants for chemical synthesis of SNP [29]. In contradiction, we used comparatively lower concentration of trisodium citrate as reducing agent and higher amount of $AgNO_3$ as optimum concentration.

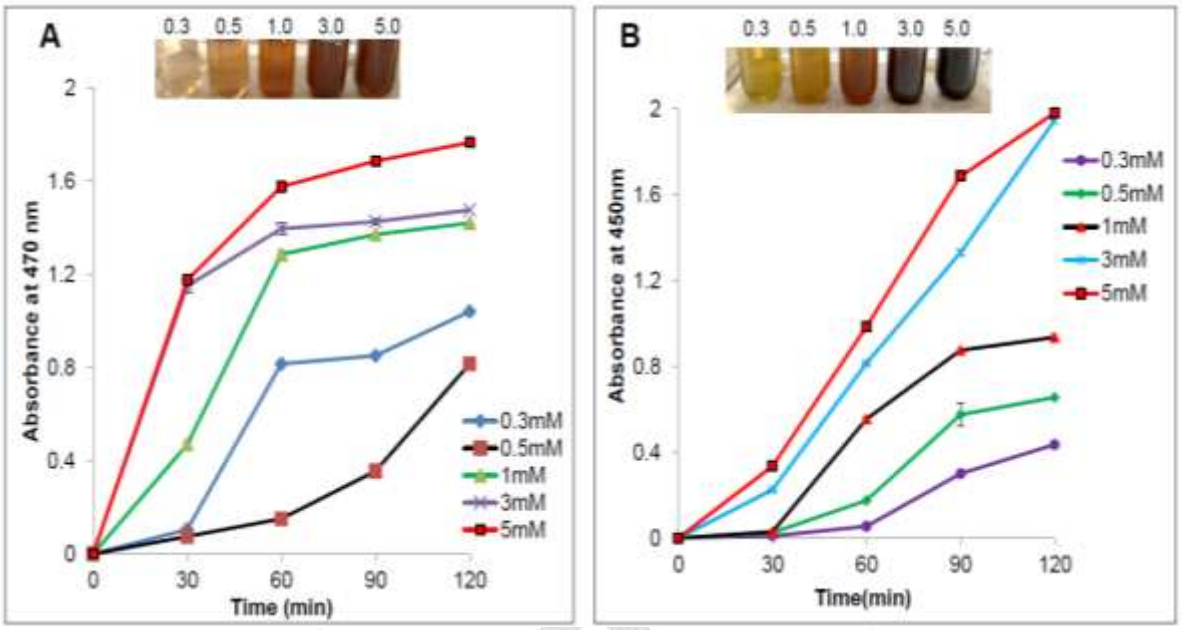

Figure 2. Optimization of $AgNO_3$ concentration for PSNPs and CSNPs. (A) Time course of PSNP synthesis at 40ºC using different concentrations of $AgNO_3$. (B) Time course of CSNP synthesis at 70ºC using different concentrations of $AgNO_3$. *Inset*: Corresponding color change in the reaction tubes.

3.2.2 Temperature

In order to determine the optimum temperature of incubation, leaf extract and trisodium citrate were mixed with 5 mM $AgNO_3$ and the tubes were incubated at different temperatures. It is clear from Figure 3A that maximum synthesis of PSNPs was obtained at 40˚C followed by a decrease in synthesis with increase in reaction temperature up to 70˚C. This could be due to the fact that the key biomolecules, present in plant extract, responsible for the reduction process are denatured or deactivated at higher temperature resulting in loss of their activity as reducing agents. In another report, synthesis of PSNPs using *M. koenigii* leaf extract was carried out at room temperature [40]. Hence, it can be said that the optimum temperature required for synthesis of PSNPs is usually low.

For CSNPs, maximum synthesis occurred when temperature of incubation was increased to 80˚C and showed complete reduction of silver ions (Figure 3B). The tubes were also incubated at higher temperatures, i.e. at 90˚C and 100˚C, which resulted in deposition of silver on walls of the tube making it difficult to take readings. Hence, 80˚C was used as the optimum temperature for synthesis of CSNPs with 5 mM $AgNO_3$. According to the study of Fang et al., trisodium citrate and $AgNO_3$ were mixed vigorously with heating for formation of SNPs [41]. It indicates that the citrate ions require high temperature to act as reducing agent.

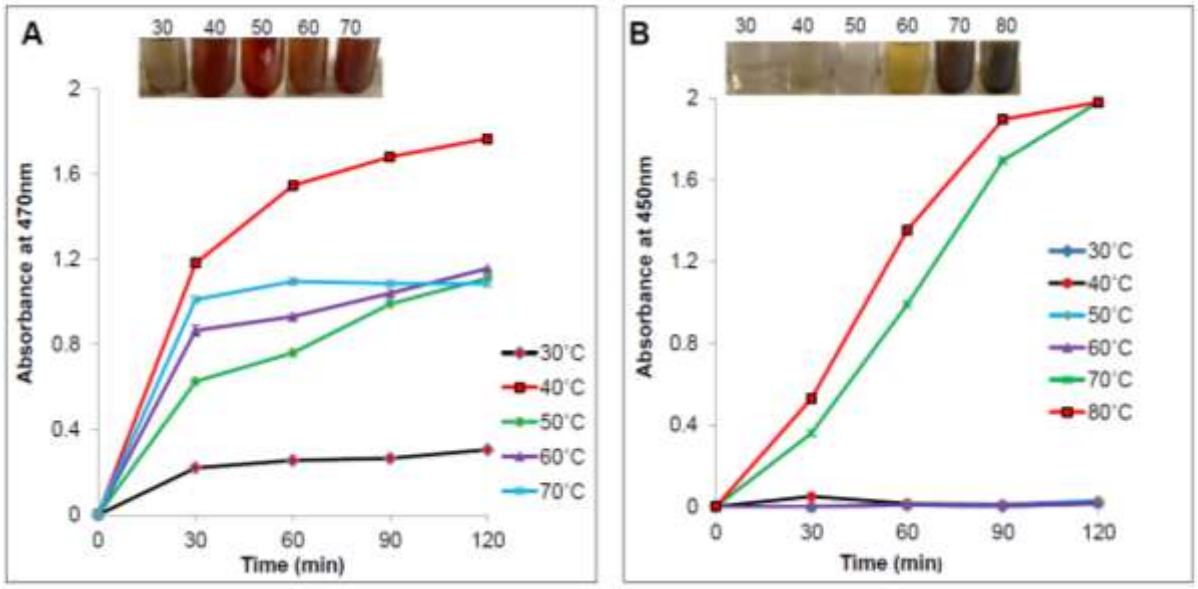

Figure 3. Optimization of temperature for PSNPs and CSNPs. (A) Time course of PSNP synthesis using 5mM $AgNO_3$ incubated at different temperatures. (B) Time course of CSNP synthesis using 5mM $AgNO_3$incubated at different temperatures. *Inset*: Corresponding color change in the reaction tubes.

3.3 Characterization of SNPs

3.3.1 UV-visible spectra analysis

UV-Vis spectroscopy is one of the important tools for characterizing SNPs through SPR and optical absorption spectra produced by metal nanoparticles [42]. As compared to the UV-visible spectrum obtained for 1 mM $AgNO_3$, a blue-shift in SPR peak from 470 to 440 nm was observed for PSNPs indicating a change in their morphology during optimization (Figure 4). Formation of small-sized SNPs has been

reported to cause the blue-shift in UV-vis spectrum [43]. According to Godet et al., a decrease in absorbance is seen due to aggregation among nanoparticles over a period of time [29]. Similar observations were reported by Singh et al. for bacteria-mediated synthesis of SNPs [28]. In case of CSNPs, no change in the location of SPR peak was observed which was obtained at 450 nm before and after optimization.

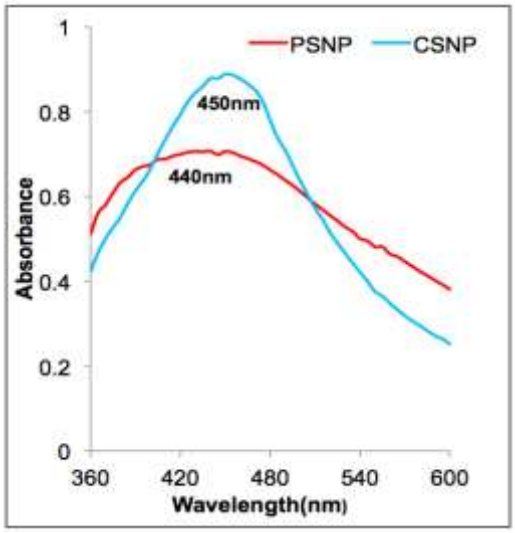

Figure 4. UV-Vis spectrum of PSNP and CSNP after optimization.

3.3.2 TEM analysis

TEM micrographs, observed at different magnifications, showed the formation of polydisperse and roughly spherical SNPs as shown in the Figure 5. SNPs predominately adopt a spherical morphology with few exceptions [28]. Size of PSNPs was between 2 to 18 nm and that of CSNPs was between 10 to 35 nm, as estimated by ImageJ software. This implies that CSNPs were larger in size as compared to PSNPs. Moreover, it was found that PSNPs were embedded inside an organic matrix. In a similar finding, PSNPs were reported to be surrounded by a thin layer of organic material from *Mangolia* leaf broth [44]. Size and aggregation state of CSNPs are affected without the use of stabilizing agent [26]. The larger particles may form due the agglomeration of smaller ones via Ostwald ripening [25]. However, in our case, CSNPs possess an overall negative charge due to citrate ions that also act as capping agent. The charge accrues a repulsive force due to which there is lesser aggregation and the particles are separated and not uniform [45].

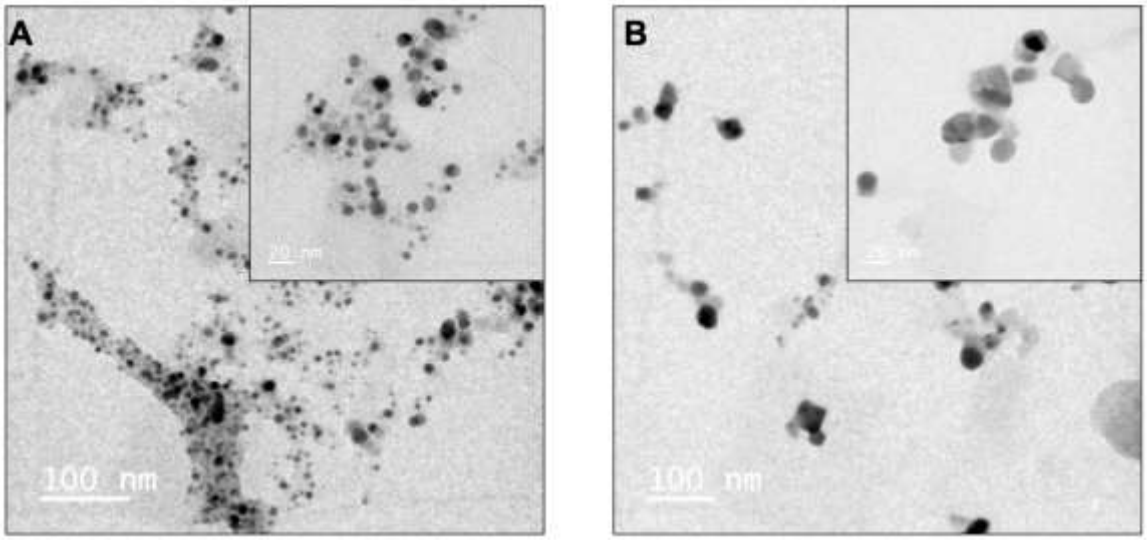

Figure 5. TEM images of (A) PSNP (B) CSNP. *Inset*: Magnified TEM image (scale ~ 20 nm)

3.3.3 SAED

The crystallinity of SNPs was detected by SAED analysis and a typical pattern is depicted in Figure 6. When the electron diffraction pattern of SNPs is carried out on limited number of crystals, one observes only some spots with concentric circles. In our study, appearance of discrete spots in ring-like diffraction pattern for both PSNPs and CSNPs proved that the majority of the particles are crystalline, as also reported earlier [44,46]. The patterns showed bright circular rings corresponding to the (111), (200), (220) and (311) planes of SNPs. The diffraction rings could be indexed on the basis of face-centered cubic (fcc) structure of silver.

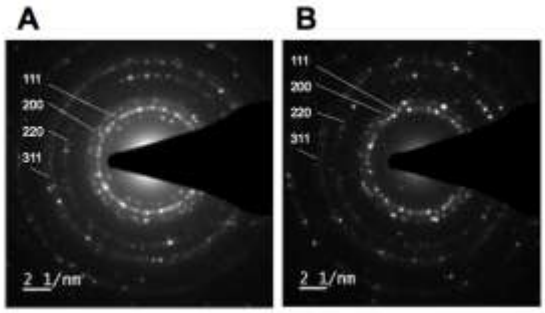

Figure 6. SAED pattern of randomly selected (A) PSNP (B) CSNP.

3.4 Screening of dyes for catalytic activity of SNPs

Catalytic activity of SNPs was evaluated using synthetic dyes, namely, crystal violet, malachite green, safranin, methylene blue, trypan blue and congo red, at a concentration of 0.05 mg/ml (Table 1). The reduction of aqueous solution of these dyes using excess of $NaBH_4$ was carried out by a method reported by Reddy et al. [47]. Out of the six dyes used in this study, only congo red and trypan blue showed immediate complete decolorization on exposure to the combination of SNPs and $NaBH_4$ whereas the tubes containing only $NaBH_4$ did not show any considerable change in color (Figure 7). This indicates that SNPs act as catalyst for $NaBH_4$ mediated reduction reaction, which makes the reaction very rapid; otherwise, that could take several months for the same. It is important to note that congo red and trypan blue belong to azo dye family. SNPs help in transfer of electron from hydride ions (donors) to azo bond (acceptors) as reported by Wadhwani et al. [6]. Methylene blue is a redox dye, which decolorized in presence of only $NaBH_4$. However, it again oxidized, in presence of oxygen, yielding a blue color. In presence of SNPs, a colored ring was formed during decolorization of safranin and methylene blue, which on mixing gave incomplete decolorization. On contrary to our observations, SNPs have been reported to decolorize methylene blue in presence of sunlight [48]. Malachite green and crystal violet showed decolorization with only $NaBH_4$ (in absence of SNPs) suggesting no catalysis is required for their decolorization reaction. No considerable effect was seen in tubes of safranin, congo red and trypan blue containing only $NaBH_4$. Control tubes containing dye and SNPs did not exhibit any effect on the solution. There are only few reports on catalytic activity of SNPs in presence of $NaBH_4$ for dye decolorization [49]. However, concentration of SNPs used was not mentioned. Besides SNPS, gold nanoparticles have been majorly used for decolorization of dyes, such as congo red and methylene blue [47].

Table 1. Decolorization of dyes (0.05 mg/ml) with SNPs (1 mg/ml) and sodium borohydride (3.5 mg/ml).

Dyes	Dye	Dye + Sodium borohydride	Dye + Sodium borohydride + SNPs	Dye + SNPs
Malachite green	-	+	+	-
Crystal violet	-	+	+	-
Safranin	-	-	+ (ring)	-
Methylene blue	-	-	+ (ring)	-
Congo red	-	-	+	-
Trypan blue	-	-	+	-

Note: decolorization (+); no decolorization (-)

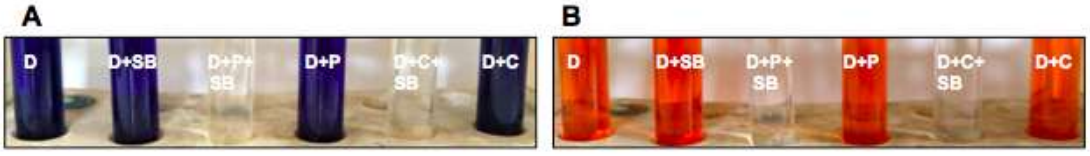

Figure 7. Complete decolorization of (A) trypan blue, and (B) congo red with sodium borohydride in presence of SNP. *Abbreviations:* D (dye); SB (sodium borohydride); P (PSNPs); C (CSNPs).

3.5 Effect of SNP concentration on dye decolorization activity

In order to determine the effect of concentration of nanocatalyst on decolorization of congo red and trypan blue, different concentrations of SNPs with 3.5 mg/ml $NaBH_4$ were used. As the concentration of nanocatalyst decreases, there is increase in time required for decolorization (Table 2). At highest concentration of 1 and 0.5 mg/ml, immediate complete decolorization was obtained. At lowest concentration of 0.001 mg/ml, trypan blue decolorized within 45 min; however, at least 120 min were required for decolorization of congo red. On a comparative note, PSNPs gave faster results as compared to CSNPs for both the dyes. In one report, Wadhwani et al reported decolorization of textile dyes, direct black and reactive yellow, with gold nanoparticles and obtained only up to 93% decolorization at the concentration of 6.5 µg/ml after 120 min [6]. On contrary, we have obtained complete decolorization of both congo red and trypan blue within 90 min at a lower concentration of 0.005 mg/ml. It has been reported that decolorization of dyes takes place very slowly in presence of only $NaBH_4$ [50]. However, no such activity was observed in present study in absence of SNPs. Thus, it can be said that SNPs are required as catalyst to trigger $NaBH_4$ to bring about decolorization of dye.

Table 2. Decolorization of congo red and trypan blue with sodium borohydride (3.5 mg/ml) in presence of different concentrations of SNPs

Concentration of SNPs (mg/ml)	Time (minutes)			
	CONGO RED		TRYPAN BLUE	
	PSNPs	CSNPs	PSNPs	CSNPs
1	Immediately	Immediately	Immediately	Immediately
0.5	Immediately	Immediately	Immediately	Immediately
0.1	3	7	2	2
0.05	5	11	2	2
0.01	15	30	6	11
0.005	31	90	17	18
0.001	120	> 120	40	44

3.6 UV-Visible spectroscopy

The combination of $NaBH_4$ and SNPs could decolorize congo red and trypan blue very rapidly, which was monitored by reading UV-visible spectrum at regular intervals. At 0.01 mg/ml concentration of SNPs, congo red took up to 30 min for decolorization, which can also be seen in the Figure 8. The absorption maximum for congo red was located at 495 nm that was seen to be declined drastically on exposure to the combination of $NaBH_4$ and SNPs. For PSNPs, the peak disappeared in 20 min while with CSNPs, it took 30 min. Similar results were obtained for trypan blue where, the peak located at initially 570 nm was observed to decrease on exposure to $NaBH_4$ and 0.005 mg/ml SNPs (Figure 9). It is important to note that a new peak of product was also observed at 375 nm. The decreasing trend in the adsorption maxima indicates reduction of dye [47]. Similar results were reported by Wadhwani et al. for decolorization of textile dyes, direct black and reactive yellow, using gold nanoparticles [6].

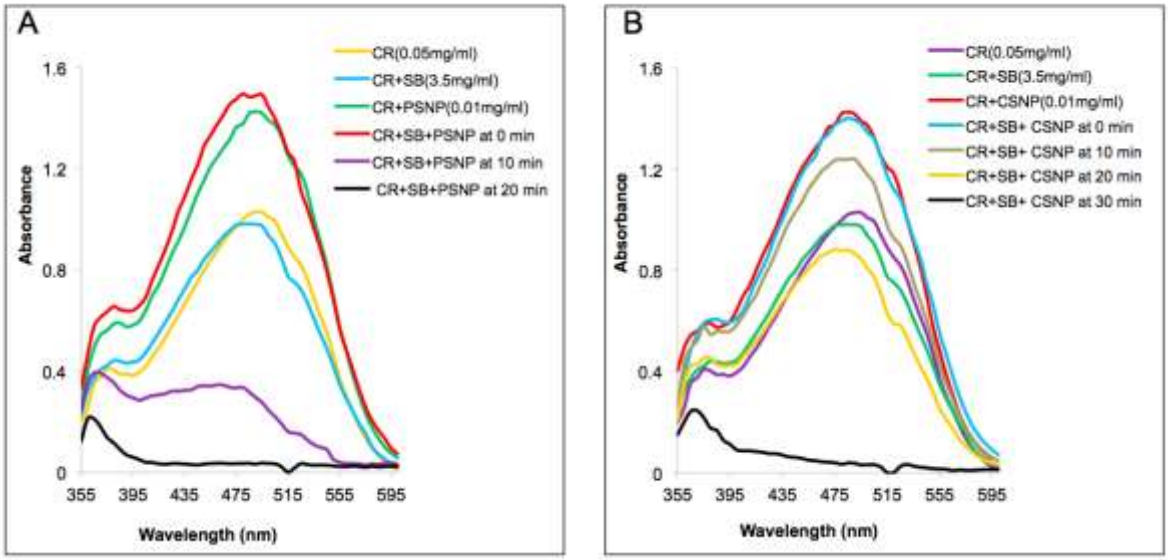

Figure 8. UV-visible spectrum of congo red at different time points during decolorization with sodium borohydride (3.5 mg/ml) and SNPs (0.01 mg/ml).

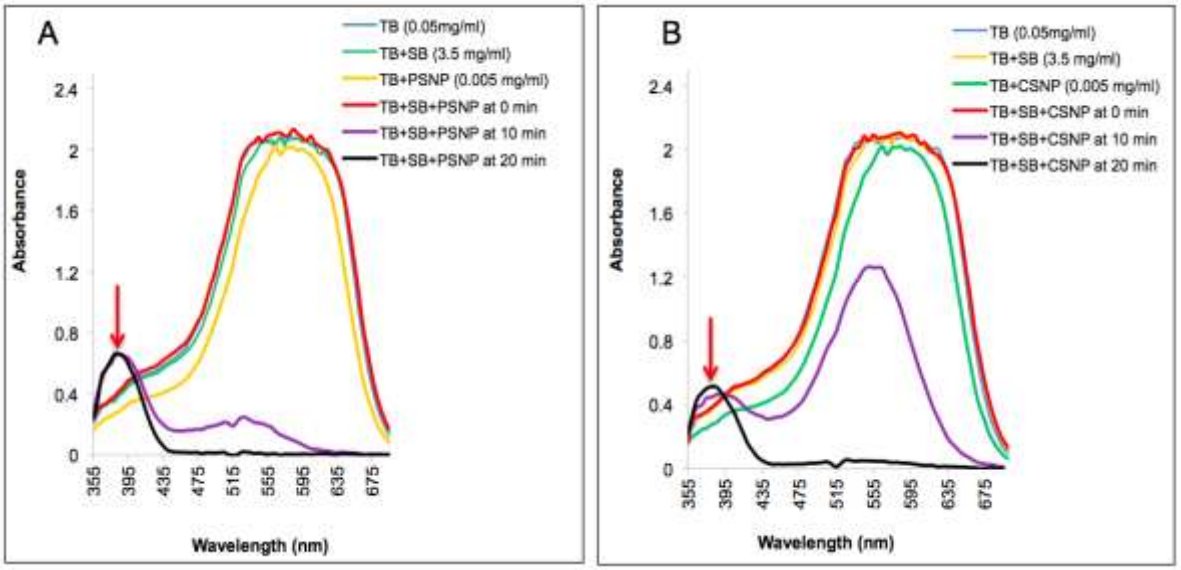

Figure 9. UV-visible spectrum of trypan blue at different time points during decolorization with sodium borohydride (3.5 mg/ml) and SNPs (0.01 mg/ml).

The azo group (-N=N-) belongs to the class of basic chromophores, which impart color to dyes. Both congo red and trypan blue are diazo dyes having two azo bonds. It was proposed that $NaBH_4$ cleaves the multi azo group leading to decolorization of dye. However, $NaBH_4$ is a weak reducing agent and requires a catalyst for its efficient action. The catalytic activity of SNPs at nanoscale is due to its reduction in redox potential to negative value; therefore, SNPs can facilitate the transfer of electrons from hydride ions to dye in the catalytic process [51]. Based on this assumption, a possible pathway for degradation of congo red and trypan blue in presence of $NaBH_4$ and SNPs has been shown in Figure 10A and 10B, respectively. However, confirmation by mass-spectrometry should be carried out.

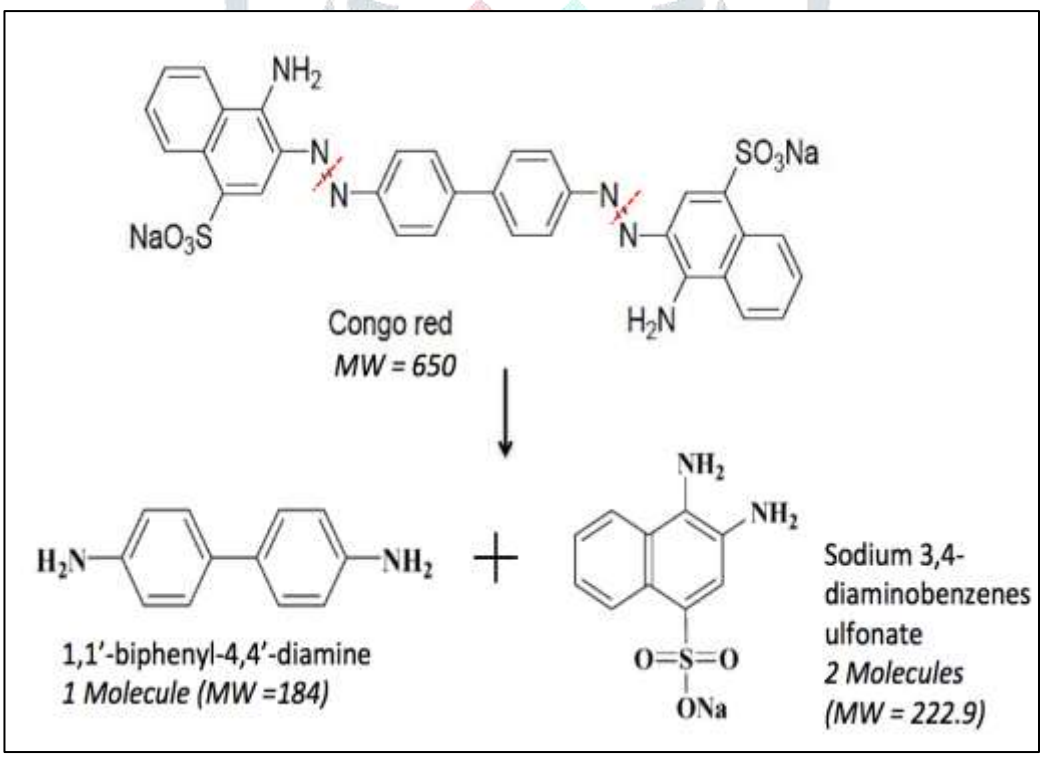

Figure 10A. Possible pathway for decolorization of congo red by sodium borohydride and SNPs.

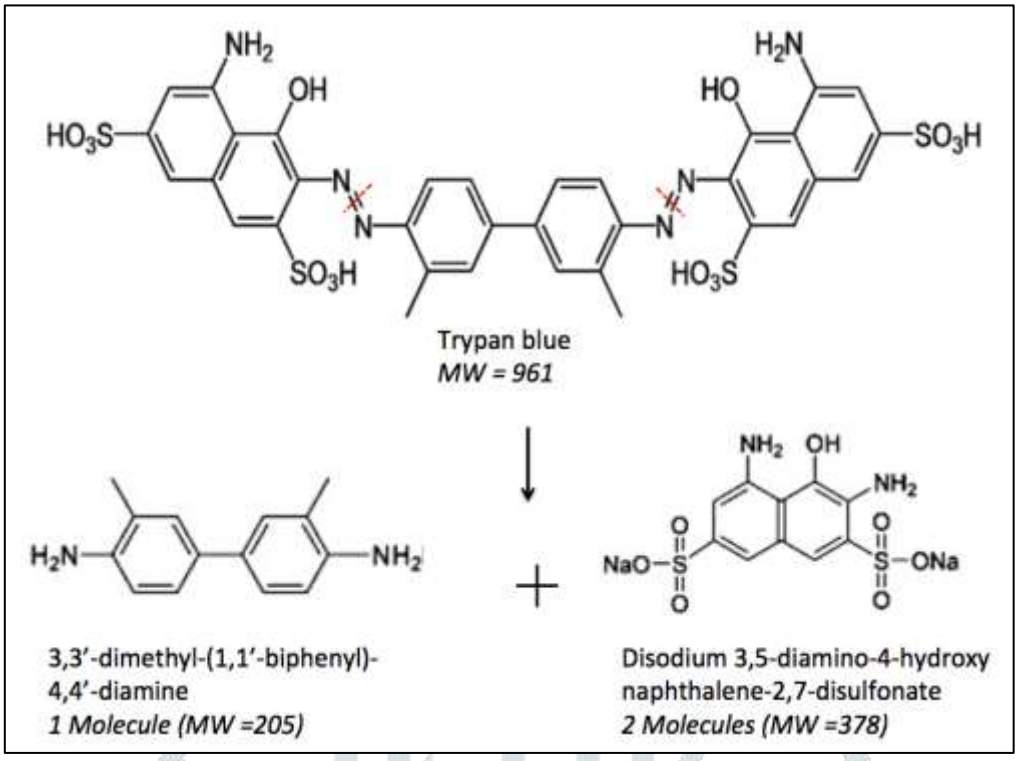

Figure 10B. Possible pathway for decolorization of trypan blue by sodium borohydride and SNPs.

In conclusion, both PSNPs and CSNPs exhibit dye decolorization activity. However, the rate was faster with PSNPs for both congo red and trypan blue. The plausible explanation for could be the difference in size. PSNPs were comparatively smaller than CSNPs, and hence, possessed higher catalytic activity. Toxicity studies with respect to dyes and their reduced products warrants further investigation.

ACKNOWLEDGMENT

Authors acknowledge the support of Sophisticated Analytical Instrument Facility (SAIF), IIT Mumbai for TEM and SAED analysis.

REFERENCES

[1] Ventura-Camargo, B. and Marin-Morales, M. 2013. Azo dyes: characterization and toxicity – a review. Textiles and Light Industrial Science and Technology, 2(2): 85-103.

[2] Kammradt, P.B. 2004. Color removal of dye from industrial effluents by oxidation process. Thesis (Master – Eng. Water and Environmental Resources), Paraná University, Curitiba, Brazil.

[3] Oliveira, D.P. 2005. Dyes as important class of environmental contaminants – a case study. Thesis (Doctor – Toxicology and Toxicological Analyses), São Paulo University, São Paulo, Brazil.

[4] Chequer, F.M.D., de Oliveira, G.A.R., Ferraz, E.R.A., et al. 2013. Textile dyes: dyeing process and environmental impact. In: Gunay, M. (ed) Eco-friendly textile dyeing and finishing. InTech Press, Crotia.

[5] Soni, H.I., Bakre, P.P. and Bhatnagar, P. 2008. Assessment of teratogenecity and embrotoxicity of sludge from textile industries at Pali (India) in Swiss albino mice exposed during organogenetic period. Journal of Environment Biology, 29(6): 965–969.

[6] Wadhwani, S.A., Shedbalkar, U.U., Nadhe, S., et al. 2018. Decolorization of textile dyes by combination of gold nanocatalyts obtained from *Acinetobacter* sp. SW30 and $NaBH_4$. Environmental Technology & Innovation, 9: 186-197.

[7] Ghosh, B.K., Hazra, S., Naik, B., et al. 2015. Preparation of Cu nanoparticle loaded SBA-15 and their excellent catalytic activity in reduction of variety of dyes. Powder Technology, 269: 371–378.

[8] Mani, S. and Bharagava, R.N. 2016. Exposure to crystal violet, its toxic, genotoxic and carcinogenic effects on environment and its degradation and detoxification for environment safety. Reviews of Environmental Contamination and Toxicology, 237: 71-104.

[9] Zare, K., Sadegh, H., Shahryari-Ghoshekandi, R., et al. 2015. Enhanced removal of toxic congo red dye using multi walled carbon nanotubes: kinetic, equilibrium studies and its comparison with other adsorbents. Journal of Molecular Liquids, 212: 266-271.

[10] Din, M.I., Hussain, Z., Mirza, M.L., et al. 2013. Biosorption of toxic congo red dye from aqueous solution by eco-friendly biosorbent *Saccharum bengalense*: kinetics and thermodynamics. Desalination and Water Treatment, 51(28-30): 5638-5648.

[11] Auerbach, S.S., Bristol, D.W., Peckham, J.C., et al. 2010. Toxicity and carcinogenicity studies of methylene blue trihydrate in F344N rats and B6C3F1 mice. Food Chemistry and Toxicology, 48(1): 169-177.

[12] Ford, R.J. and Becker, F.F. 1982. The characterization of trypan blue-induced tumors in Wistar rats. The American Journal of Pathology, 106(3): 326-331.

[13] Sahu, M.K., Sahu, U.K. and Patel, R.K. 2015. Adsorption of safranin-O dye on CO2 neutralized activated red mud waste: process modeling, analysis and optimization using statistical design. RSC Advances, 5, 42294-42304.

[14] Bhosale, M.A. and Bhanage, B.M. 2015. Silver nanoparticles: synthesis, characterization and their application as a sustainable catalyst for organic transformations. Current Organic Chemistry, 19(8): 708-727.

[15] Gowri, R.S., Vijayaraghavan, R. and Meenambigai, P. 2014. Microbial degradation of reactive dyes- A Review. International Journal of Current Microbiology and Applied Sciences, 3(3): 421–436.

[16] Kurtan, U., Baykal, A. and Soz¨eri, H. 2015. Recyclable Fe_3O_4@tween20@Ag nanocatalyst for catalytic degradation of azo dyes.

Journal of Inorganic and Organometallic Polymers, 25: 921–929.

[17] Xua, L., Li, X., Ma, J., et al. 2014. Nano-MnOx on activated carbon prepared by hydrothermal process for fast and highly efficient degradation of azo dyes. Applied Catalysis A:General, 485: 91–98.

[18] Saha, S., Anjali, P., Subrata, K., et al. 2010. Photochemical green synthesis of calcium-alginate-stabilized Ag and Au nanoparticles and their catalytic application to 4-Nitrophenol reduction. Langmuir, 26(4): 2885–2893.

[19] Narayanan, R. 2012. Synthesis of green nanocatalysts and industrially important green reactions. Green Chemistry Letters and Reviews, 5(4): 707–725.

[20] Pradhan, N., Pal, A. and Pal, T. 2001. Catalytic reduction of aromatic nitro compounds by coinage metal nanoparticles. Langmuir, 17: 1800–1802.

[21] Jiang, Z.J., Liu, C. Y. and Sun, L.W. 2005. Catalytic properties of silver nanoparticles supported on silica spheres. Journal of Physical Chemistry B, 109(5): 1730-1735.

[22] Wang, J., Liu, J., Guo, X., et al. 2016. The formation and catalytic activity of silver nanoparticles in aqueous polyacrylate solutions. Frontiers of Chemical Science and Engineering, 10(3): 432-439.

[23] Saha, J., Begum, A., Mukherjee, A., et al. 2017. A novel green synthesis of silver nanoparticles and their catalytic action in reduction of methylene blue dye. Sustainable Environment Research, 27(5): 245-250.

[24] Singh, R., Shedbalkar, U.U., Wadhwani, S.A., et al. 2015. Bacteriagenic silver nanoparticles: synthesis, mechanism, and applications. Applied Microbiology and Biotechnology 99: 4579-4593.

[25] Cushing, B.L., Kolesnichenko, V.L. and O'Connor, C.J. 2004. Recent advances in the liquid-phase synthesis of inorganic nanoparticles. Chemical Reviews, 104: 3893-3946.

[26] Dang, T.M., Le, T.T., Blance, E.F., et al. 2012. Influence of surfactant on the preparation of silver nanoparticles by polyol method. Advances in Natural Sciences: Nanoscience and Nanotechnology, 3:1-4.

[27] Ghosh, S., Patil, S., Ahire, M., et al. 2012. Synthesis of silver nanoparticles using *Dioscorea bulbifera tuber* extract and evaluation of its synergistic potential in combination with antimicrobial agents. International Journal of Nanomedicine 7:483.

[28] Singh, R., Wagh, P., Wadhwani, S., et al. 2013. Synthesis, optimization, and characterization of silver nanoparticles from *Acinetobacter calcoaceticus* and their enhanced antibacterial activity when combined with antibiotics. International Journal of Nanomedicine 8: 4277.

[29] Godet, S., Maribel, G., Dille, J., et al. 2009. Synthesis of silver nanoparticles by chemical reduction method and their antibacterial activity. International Journal of Chemical and Biomolecular Engineering, 2: 24-26.

[30] Singh, R., Shedbalkar, U.U., Nadhe, S.B., et al. 2017. Lignin peroxidase mediated silver nanoparticle synthesis in Acinetobacter sp. AMB Express,7: 226.

[31] Sharma, V.K., Yngard, R.A. and Lin, Y. 2008. Silver nanoparticles: green synthesis and their antimicrobial activities. Advances in Colloid and Interface Science, 145: 83-96.

[32] Jain, V., Momin, M. and Laddha, K. 2012. *Murraya koenigii*: an updated review. International Journal of Ayurvedic and Herbal Medicine 2: 607-627.

[33] Pillai, Z.S. and Kamat, P.V. 2004. What factors control the size and shape of silver nanoparticles in the citrate ion reduction method? The Journal of Physical Chemistry B, 108: 945-951.

[34] Nath, S.S., Chakdar, D. and Gope, G. 2007. Synthesis of CdS and ZnS quantum dots and their applications in electronics. Nanotrends, 2: 20-28.

[35] Henglein, A. 1993. Physiochemical properties of small metal particles in solution: microelectrode reactions, chemisorption, composite metal particles and the atom-to-metal transition. Journal of Physical Chemistry B, 97: 5457-5471.

[36] Shrivastava, S. and Dash, D. 2010. Label-free colorimetric estimation of proteins using nanoparticles of silver. Nano-Micro Letters, 2: 164-168.

[37] Novak, J.P. and Feldhein, D.L. 2000. Assembly of phenylacetylene bridged silver and gold nanoparticle arrays. Journal of the American Chemical Society, 122: 3979-3980.

[38] Natrajan, K., Selvaraj, S. and Murty, V.R. 2010. Microbial production of silver nanoparticles. Digest Journal of Nanomaterials and Biostructures, 5: 135-140.

[39] Bhandari, P.R. 2012. Curry leaf (*Murraya koenigii*) or cure leaf: review of its curative properties. Journal of Medical Nutrition and Nutraceuticals, 1: 92.

[40] Sajeshkumar, N.K., Jose, P.V., Mathew, J.J., et al. 2015. Synthesis of silver nanoparticles from curry leaves (*Murraya koenigii)* extract and its antibacterial activity. CIBTech Journal of Pharmaceutical Sciences, 4: 2319-3891.

[41] Fang, J., Zhang, C. and Mu, R. 2005. The study of silver particulate films by simple method for efficient SERS. Chemical Physics Letters, 401: 271-275.

[42] Jain, P.K., Huang, X., El-Sayed, I.H., et al. 2007. Review of some interesting surface plasmon resonance-enhanced properties of noble metal nanoparticles and their applications to biosystems. Plasmonics, 2: 107-118.

[43] Petit, C., Lixon, P. and Pileni, M.P. 1993. In situ synthesis of silver nanocluster in AOT reverse micelles. Journal of Physical Chemistry A, 97: 12974-12983.

[44] Song, J.Y. and Kim, B.S. 2009. Rapid biological synthesis of silver nanoparticles using plant leaf extracts. Bioprocess and Biosystems Engineering, 32: 79-84.

[45] Landage, S.M., Wasif, A.I. and Dhuppe, P. 2014. Synthesis of nanosilver using chemical reduction methods. International Journal of Advanced Research in Engineering and Applied Sciences, 3: 11-29.

[46] Omprakash, V. and Shradha, S. 2014. Green synthesis and characterization of silver nanoparticles and evaluation of their antibacterial activity using *Elettaria Cardamon* seeds. Journal of Nanomedicine & Nanotechnology, 6: 266.

[47] Reddy, B.G., Alle, M., Dadigala, R., et al. 2015. Catalytic reduction of methylene blue and congo red dyes using green synthesized gold nanoparticles. International Nano Letters, 5: 215-222.

[48] Anandan, S., Kumar, P.S., Pugazhenthiran, N., et al. 2008. Effect of loaded silver nanoparticles on TiO_2 for photocatalytic degradation of acid red 88. Solar Energy Materials and Solar Cells, 92: 929-937.

[49] Edison, T.J.I. and Sethuraman, M.G. 2012. Instant green synthesis of silver nanoparticles using *Terminalia chebula* fruit extract and evaluation of their catalytic activity on reduction of methylene blue. Process Biochemistry, 57: 1351-1357.

[50] Kolya, H., Maiti, P., Pandey, A., et al. 2015. Green synthesis of silver nanoparticles with antimicrobial and azo dye congo red degradation properties using *Linn* leaf extract. Journal of Analytical Science and Technology 6: 33.

[51] Narayanan, K.B. and Park, H.H. 2015. Homogenous catalytic activity of gold nanoparticles synthesized using *Brassica rapa* (turnip) leaf extract in the reductive degradation of cationic azo dye. Korean Journal of Chemical Engineering, 32: 1273-1277.